DAMAGE QUANTIFICATION IN METAL MATRIX COMPOSITES

G. Z. VOYIADJIS, A. R. VENSON, and R. K. ABU-ALRUB
Department of Civil and Environmental Engineering
Louisiana State University
Baton Rouge, LA 70803

Abstract

An experimental procedure is presented to quantify damage in terms of microcrack density. This is accomplished by experimentally evaluating the components of a second-order damage tensor for a metal matrix composite material. The procedure involves the use of a scanning electron microscope and image analyzing software to quantify physical damage features found on a representative volume element. These features are quantified in terms of crack density, which is used in developing the second-order damage tensor. This procedure is applied to a titanium aluminide SiC-reinforced laminate. Laminates of the following staking sequences, $(0/90)_S$ and $(\pm 45)_S$, are tested under uniaxial tensile loadings. Damage evolution is obtained by loading the specimens over a range of load intensities from rupture load down to 70% rupture load. A proposed formulation for a coupled anisotropic damage model for the inelastic response of composite materials is presented in this work.

1. Introduction

Various theoretical models exist for investigating the effects of damage on metal matrix composites. Limited experimental investigations have been performed to relate physical damage to a corresponding theoretical definition. These investigations are primarily confined to damage as a result of fatigue and or fracture [1], with little correspondence between physical and theoretical damage. Additionally, these investigations do not present the damage evolution in terms of a function of the measured physical damage over the load history. In a recent publication, [2] presented a thorough examination and explanation of the microstructural evolution of damage. The work from their investigation still needs to be incorporated into a constitutive theory for the quantification and evolution of physical damage. Other more recent experimental procedures have also been introduced to quantify damage due to microcracks and microvoids through X-ray diffraction, tomography, and so forth [3]. However, these procedures are in need of refinement that will allow the ease of differentiating different types of damage such as voids and cracks (radial, debonding, and z-type).

E.E. Gdoutos (ed.), Recent Advances in Experimental Mechanics, 109–120.

Although some steps have been taken to correlate physical and damage and its theoretical definition, additional experiments are needed to quantify damage parameters and evaluate the corresponding damage theory. The work that has been done uses a continuum definition with various schemes to measure damage. These schemes measure damage as a ratio between an effective quantity and its respective damage value. [4] listed several such schemes that defined the damage parameter ratio based on the area of resistance, material density, or elastoplastic modulus, among others. The ratio defined by the elastoplastic modulus is commonly used to obtain the damage parameter due to the ease in evaluating the damaged and undamaged elastoplastic moduli.

The material presented in this work will outline a technique to experimentally evaluate different types of damage in a metal matrix composite material. It will also show how the resulting damage parameters can be incorporated into a micromechanical damage theory. The focus of the technique presented is in support of an elastoplastic micromechanical damage model developed in [5] and [6]. However, the results of this work can be used with any damage theory based on a tensorial damage parameter.

2. Design and Manufacture of Specimens

The material investigated is a titanium aluminide composite reinforced with continuous SiC (SCS-6) fibers. Typical properties of the SiC fibers are shown in Table 1. It is reported that these fibers have good wettability characteristics for metals, which minimizes the chance of voids being induced during the manufacturing process. These fibers are also coated with a carbon rich coating that assists in protecting the inner SiC from damage during handling. Both of these features are important in reducing the opportunity for inducing damage during manufacturing.

TABLE 1. Typical Properties of Silicon Carbide Fibers.

Parameter	Value
Diameter	0.14 mm
Density	3044.00 kg/mm^3
Tensile strength	3.44 Gpa
Young's modulus	414.00 Gpa
Poisson ratio	0.22
CTE	2.30 X 10^{-6} ppm – °C at RT

Note: Provided by Textron Specialty Materials, Inc. Lowell, MA USA.

The matrix material originates as a titanium aluminide foil in an α_2 phase, with typical properties as shown in Table 2. The titanium aluminide foil is made from rolled ingot material. Niobium is added to the matrix to improve overall composite ductility [7]. Material properties of a composite lamina for 0° and 90° orientations were obtained from experimental tests. These values are as reported in Table 3.

TABLE 2. Typical Properties of Ti – 14Al – 21Nb α_2 Matrix.

Parameter	Value
Composition= Ti	63.40%
Composition= Al	14.40%
Composition= Nb	22.10%
Tensile strength	448.00 MPa
Young's modulus	84.10 GPa
Poisson ratio	0.30

Note: Provided by Textron Specialty Materials, Inc. Lowell, MA USA

TABLE 3. Typical Properties of SiC – Ti – Al Lamina

Parameter	Value
0° tensile strength	1.38 – 1.52 Gpa
90° tensile strength	103.00 – 206.00 MPa
Longitudinal modulus	199.00 Gpa
Transverse modulus	136.00 Gpa
Shear modulus, G_{12}	52.40 Gpa
Poisson ratio (ν_{12})	0.270
Poisson ratio (ν_{21})	0.185
Poisson ratio (ν_{31})	0.310

Note: Provided by Textron Specialty Materials, Inc. Lowell, MA USA

Two 304.80 × 304.80 mm plates with layups of $(0/90)_S$ and $(\pm 45)_S$ are fabricated using hand layup techniques from SCS – 6 SiC fiber mats and Ti – 14A1 – 21Mb α_2 foils. Each of the plates contained four plies with a 0° or +45° as the top and bottom ply for the respective layups. Fibers are included in each ply in the form of a fiber mat, were fibers are held together with molybdenum wires. This mat aide in keeping the fibers aligned and equally spaced during the consolidation process. Consolidation was accomplished by hot-isostatic-pressing (HIP) in a steel vacuum bag at 1010 °C ±25° under 103.00 MPa pressure for 2 hrs. The most severe warpage, resulting from the differences in coefficients of thermal expansion for the fiber and matrix, was confined to the edges of each plate, with a maximum relative elevation difference of 2.24 cm for the $(0/90)_S$ plate and 1.30 cm for the $(\pm 45)_S$ plate. Care is taken during specimen preparation to ensure that this warpage does not induce damage. Each of the laminates was machined using diamond tooling to produce six tensile test specimens with shape of dogbone type specimen. The shape of the dogbone type specimen was selected based on a successful use by previous researchers [8]. This shape will ensure specimen failure within the gage section and not the grips. Aluminum tabs are arc-welded onto the ends of each test specimen in order to prevent the mechanical grips from damaging the specimen.

3. Tensile Testing of Specimens

The experimental model used was designed to collect quantitative and qualitative data. Recommendations for specimen preparation suggested in [9] were used in determining the method and procedure needed to collect quantitative data. It was decided to use foil-resistance strain gages to collect the quantitative strain data. Placement of strain gages follows the recommendations suggested in [10]. Each of the dogbone type specimens contained a transverse and longitudinal strain gage pair mounted on the top and bottom surfaces. Mechanical testing is done utilizing a computer controlled load frame with hydraulic grips. The material tested failed at a maximum load of 5.23 kN and 8977 $\mu\epsilon$. Since these maximum were at such low levels, specimens are loaded at a crosshead rate of 4.23 mm/hr to allow enough time to collect sufficient data during the test. A personal computer was used to control the load frame as well as the data acquisition system. This allowed data to be sampled continuously without interrupting the test. Calibration factors were obtained for all specimen strain gages before testing and used later during data reduction. Immediate feedback of load *vs* strain was obtained by attaching an extensometer to the specimen with results being plotted on an oscilloscope while the test was being run. Results from the extensometer matched within ±3% the longitudinal results of the strain gages. One dogbone type test specimen from each laminate layup is loaded to rupture. The remaining five specimens are loaded to 90, 85, 80, 75 and 70% of rupture load. By loading specimens to different load levels a measure of the evolution of damage through the progression of loading can be obtained. The actual quantification of damage is obtained by measuring damage features on a representative cross section. Load *vs* longitudinal %strain curves for selected dogbone shaped specimens of orientations $(0/90)_S$ and $(\pm 45)_S$ are shown in Figures 1 and 2, respectively.

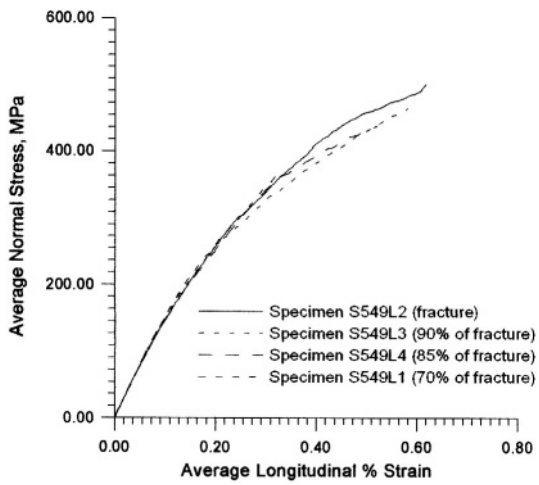

Figure 1. Normal Stress-Longitudinal %strain curves for selected $(0/90)_S$ specimens.

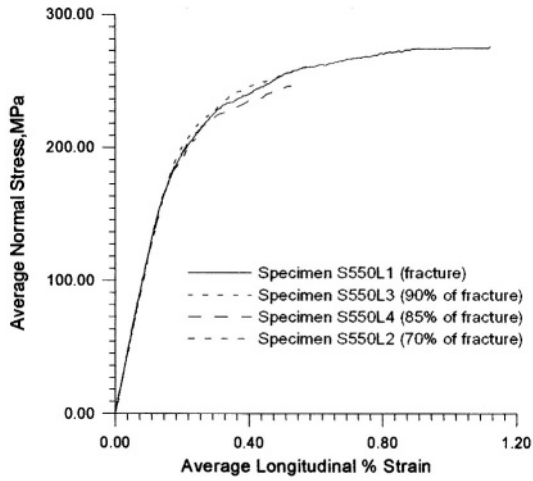

Figure 2. Normal Stress-Longitudinal %strain curves for selected $(\pm 45)_S$ specimens.

4. SEM Analysis and Damage Quantification of Specimens

Following mechanical testing, all specimens were sectioned into small samples for further investigation using image analysis. The purpose of the image analysis is to identify and quantify all damage features that may exist on the cross section of the sample. Results of information collected are then compiled for characterization of damage. Details of the complete procedure and results are given in the following paragraphs.

A scanning electron microscope was used to perform an SEM analysis of a representative cross section of all specimens to obtain qualitative information. Photographs are also taken during this analysis so that the visible damage features can be measured later using image processing software. Longitudinal and transverse sections are taken from all samples in the vicinity of the strain gages. The transverse cross-sections contained a portion of the free edge. In order to eliminate any possible free edge effects, information within two fiber diameters of the specimen free edge is disregarded. Since the longitudinal cross sections are carefully taken from the middle of the specimen, free edge effects did not have to be considered. All SEM samples were cut from the original test specimen using a low speed diamond saw. The low speed diamond saw eliminates the possibility of introducing damage on the cross section during sectioning. In addition, the cut surfaces were ground and polished to eliminate any surface defects that can be introduced by the cutting operation. Careful observance of this procedure increases the probability that defects observed during the SEM analysis reflect damage as a result of the loading only. Although, the cross section could contain radial cracks as a result of the fabrication cool down process, it is assumed that a well-controlled manufacturing process was used such that the number of these cracks is low and can be neglected. Therefore, all measured cracks are attributed to loading.

The entire cross-sectional areas of the longitudinal and transverse sections are scanned at low magnification (<1000X). Based on the observations of this analysis, photographs are taken on an area of the cross section that is 1% of the total area and contains an average representation of damage features for the complete cross-section. The aforementioned area is taken as one of the three mutually perpendicular planes used in defining the representative volume element (RVE). Similar areas were considered on the remaining mutually perpendicular sample sections to complete the planes of the RVE.

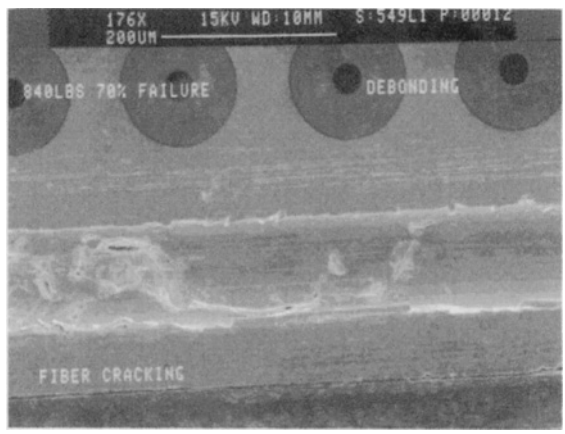

Figure 3. SEM photo of $(0/90)_S$ specimen at 70% of failure load showing fiber cracking.

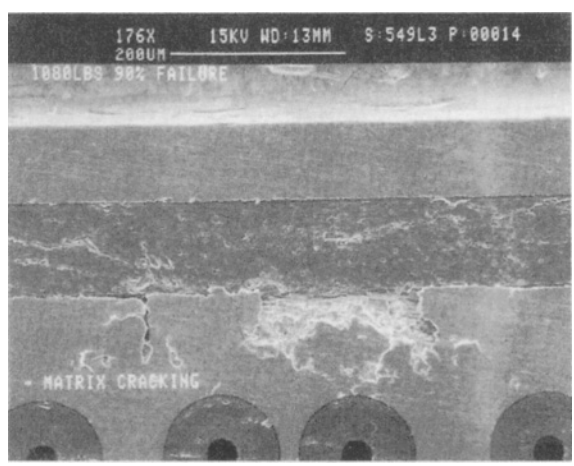

Figure 4. SEM photo of $(0/90)_S$ specimen at 90% of failure load showing matrix cracking.

Results of the SEM analysis showed a higher occurrence of damage in the fibers than in the matrix. The type of damage was mainly confined to cracks in the fiber or in the matrix material adjacent to the fiber/matrix interface. The prevalence of the linear crack damage feature is somewhat expected, since the matrix is ductile and the fibers are very brittle. Because of the low strains obtained and the ductile nature of the matrix, damage features such as matrix voids are not expected and are not observed on any section. A sample of the damage features found on the longitudinal face of specimens investigated is shown in Figures 3 and 4. Similar damage features were found on transverse sections.

Crack length quantification was obtained through use of SEM equipment and software. The SEM photographs collected during the image analysis were scanned at a resolution of 600 dots per inch (dpi). A semi-automatic technique is used to measure crack lengths in that the cracks are digitized by hand before being processed with the image analyzing software. This software automatically computed the crack lengths with respect to the photograph scale. Information collected during the SEM and image analysis process must be related to a damage parameter that can be incorporated into a constitutive model. [5] and [6] developed a damage model that defines a second order tensorial damage parameter, $\boldsymbol{\phi}$. One of the difficulties in using this model is being able to evaluate components of the damage tensor.

In this work it is postulated that the area reduction due to damage in the effective configuration is essentially due to the development of micro cracks during the process of loading. The measure of micro crack damage, $\boldsymbol{\phi}$ is postulated to be $\boldsymbol{\phi} = \bar{\boldsymbol{\rho}} \otimes \bar{\boldsymbol{\rho}}$, in terms of the crack density, $\boldsymbol{\rho}$. Damage for an elasto-plastic response is evaluated by defining the damage tensor, $\boldsymbol{\phi}$, as a function of crack density, $\boldsymbol{\rho}$ ([7]; [11]; and [12]). For off axis laminates, the general matrix representation of $\boldsymbol{\phi}$ in terms of $\boldsymbol{\rho}$ is given as

$$[\phi] = \begin{bmatrix} \bar{\rho}_x \bar{\rho}_x & \bar{\rho}_x \bar{\rho}_y & \bar{\rho}_x \bar{\rho}_z \\ \bar{\rho}_y \bar{\rho}_x & \bar{\rho}_y \bar{\rho}_y & \bar{\rho}_y \bar{\rho}_z \\ \bar{\rho}_z \bar{\rho}_x & \bar{\rho}_z \bar{\rho}_y & \bar{\rho}_z \bar{\rho}_z \end{bmatrix} \tag{1}$$

Crack density, $\boldsymbol{\rho}$, is normalized $(\bar{\boldsymbol{\rho}})$ in equation (1) to smooth out the slight variability in evaluating crack density. The components of $\bar{\boldsymbol{\rho}}$ (i.e. $\bar{\rho}_i$; $i = x, y, z$ where x-parallel to the load axis, y-transverse to the load axis and z-normal to the xy plane) represent the normalized crack density on a cross section whose normal is along the i-axis. The off diagonal terms in equation (1) capture damage due to the interaction of cracks on the three mutually perpendicular planes of the RVE. These terms also imply that shearing stresses impose this interactive damage. Information collected during the image analysis process is used in evaluating the normalized crack density defined as,

$$\bar{\rho}_i = \frac{\rho_i}{m\rho^*}, \qquad \rho_i = \frac{l_i}{A_i} \tag{2}$$

Total crack length on the i^{th} cross-section is represented by the quantity l_i in equation (2) and A_i is the corresponding cross sectional area, m represents a normalization factor chosen so that the values of the damage variable, ϕ_{ij}, falls within the range $0 \leq \phi_{ij} < 1$. Normally the magnitude of this quantity will be 1 or close to land the term ρ^* is an expression selected such that it will yield a dimeusiouless average value for the $\overline{\rho}_i$. One possible form for ρ^* is given by

$$\rho^* = \sqrt{\rho_{x_{max}}^2 + \rho_{y_{max}}^2 + \rho_{z_{max}}^2} \tag{3}$$

where $\rho_{i_{max}}$ $(i = x, y, z)$ represents the maximum crack density of all load levels. In the case of uniaxial tension, this maximum value corresponds to the crack density evaluated at the maximum load before macrocrack initiation. $\overline{\rho}_i$ is a dimensionless quantity while ρ_i, has the dimensions of mm/mm^2.

Crack densities, are tabulated at the five load levels below rupture for each of the specimen orientations used in this investigation ([11]; [12]). Results are given in Tables 4 and 5.

TABLE 4. Overall Crack densities for $(0/90)_S$ laminate

%Load	%Strain	ρ_x X 10^{-4} (mm/mm^2)	ρ_y X 10^{-4} (mm/mm^2)
70	.3182	41.82	3.41
75	.4487	70.32	36.40
80	.4611	100.77	-
85	.5202	106.24	56.43
90	.5808	126.68	67.72

TABLE 5. Overall Crack densities for $(\pm 45)_S$ laminate

%Load	%Strain	ρ_x X 10^{-4} (mm/mm^2)	ρ_y X 10^{-4} (mm/mm^2)
70	.2414	49.23	-
75	.2779	49.32	42.44
80	.4324	51.84	101.29
85	.5268	52.99	117.01
90	.5729	56.67	146.59

These values are the crack densities computed with equation (3). Densities on the z-section are not measured and assumed to be one half the magnitude of those on the respective y-section. This assumption is made for convenience and in future damage investigations the z-plane damage should be measured. Using equation (2) and the tabulated information, the components of the damage tensor given by equation (1) for each laminate layup at 90% of the rupture load are computed as

$$[\phi] = \begin{bmatrix} 0.7368 & 0.3939 & 0.1969 \\ 0.3939 & 0.2106 & 0.1053 \\ 0.1969 & 0.1053 & 0.0526 \end{bmatrix}_{(0/90)_S}^{90\%} \tag{4}$$

$$[\phi] = \begin{bmatrix} 0.1068 & 0.2762 & 0.1318 \\ 0.2762 & 0.7145 & 0.3573 \\ 0.1318 & 0.3573 & 0.1786 \end{bmatrix}_{(\pm 45)_S}^{90\%} \tag{5}$$

similarly the damage tensor, ϕ_{ij}, for each laminate layup at different %load of the rupture can be computed. Damage parameter curves for each component of the damage tensor as a function of the strain have the same general shape as those presented in [11]; and [12]. Each of the curves shown has a concave shape with a vertical asymptote as a critical damage value is approached. The shape and form of these curves are consistent with the theoretically generated curves of [5].

5. Damage Tensor as an Internal State Variable

The anisotropic phenomenon of the microcracks distribution in the material can be interpreted using the second-order damage tensor, ϕ_{ij}, as an internal state variable of thermodynamics of irreversible processes. It is expressed as [6]:

$$\phi_{ij} = \sum_{k=1}^{3} \hat{\phi}_k n_i^k n_j^k \tag{6}$$

where $\hat{\phi}_k$ are the principal values of the damage tensor and n_i are the principal directions.

The linear elastic constitutive equation for the damaged material is written according to the principal of strain energy equivalence between the virgin material and damaged material. That is, the damaged material is modeled using the constitutive laws of the effective undamaged material in which the Cauchy stress tensor, σ_{ij}, is replaced by the effective stress tensor, $\bar{\sigma}_{ij}$, and the strain tensor, ε_{ij}, is replaced by the effective strain tensor, $\bar{\varepsilon}_{ij}$ [6]:

$$\bar{\sigma}_{ij} = M_{ijkl}\sigma_{kl} \text{ and } \bar{\varepsilon}_{ij} = M_{ijkl}^{-1}\varepsilon_{kl} \tag{7}$$

where M_{ijkl} is a fourth order damage effect tensor defined as:

$$M_{ikjl} = (\delta_{ik} - \phi_{ik})^{-1/2} (\delta_{jl} - \phi_{jl})^{-1/2} \tag{8}$$

where δ_{ij} is the Kronecker delta.

The free energy here is expressed as follows:

$$\Psi = \Psi\left(\varepsilon_{ij}^{e}, \alpha_{ij}, p, \phi_{ij}\right) \tag{9}$$

where α_{ij} and p are the flux related to the kinematic hardening and the cumulative plastic strain related to the isotropic hardening in plasticity. Assuming small elastic strains in equation (9), the average strain tensor, ε_{ij}, is decomposed into two parts: the elastic part, ε_{ij}^{e}, and the plastic part, ε_{ij}^{p}. Using the Clausus-Duhem inequality [8] one obtains:

$$\sigma_{ij} = \rho\frac{\partial\Psi}{\partial\varepsilon_{ij}^{e}}; \quad Y_{ij} = \rho\frac{\partial\Psi}{\partial\phi_{ij}}; \quad X_{ij} = \rho\frac{\partial\Psi}{\partial\alpha_{ij}}; \quad R = \rho\frac{\partial\Psi}{\partial p} \tag{10}$$

where ρ is the material density and Y_{ij}, X_{ij}, and R are the thermodynamic forces conjugate to ϕ_{ij}, α_{ij}, and p, respectively.

Assuming the decoupling between the plastic and damage dissipation processes, one can define the dissipation process as the sum of the product of the associated variable with the respective conjugate force as follows:

$$\Pi = \Pi^{p}(\dot{\varepsilon}_{ij}^{p}, \dot{\alpha}_{ij}, \dot{p}) + \Pi^{d}(\dot{\phi}_{ij}) = \sigma_{ij}\dot{\varepsilon}_{ij}^{p} - X_{ij}\dot{\alpha}_{ij} - R\dot{p} + Y_{ij}\dot{\phi}_{ij} \tag{11}$$

The rate of the internal stat variables associated with plastic and damage deformations are obtained by utilizing the calculus of function of several variables with the Lagrange multipliers $\dot{\lambda}^{p}$ and $\dot{\lambda}^{d}$, respectively, as follows:

$$\Omega = \Pi - \dot{\lambda}^{p}F^{p} - \dot{\lambda}^{d}F^{d} \tag{12}$$

Extremizing the function Ω we obtain:

$$\dot{\varepsilon}_{ij}^{p} = \dot{\lambda}^{p}\frac{\partial F^{p}}{\partial\sigma_{ij}}; \quad \dot{\alpha}_{ij} = \dot{\lambda}^{p}\frac{\partial F^{p}}{\partial X_{ij}}; \quad \dot{p} = \dot{\lambda}^{p}\frac{\partial F^{p}}{\partial R}; \quad \dot{\phi}_{ij} = \dot{\lambda}^{d}\frac{\partial F^{d}}{\partial Y_{ij}} \tag{13}$$

where $\dot{\lambda}^{p}$ and $\dot{\lambda}^{d}$ are determined using the consistency conditions $dF^{p} = 0$ and $dF^{d} = 0$, respectively.

Once a material is damaged, further loading can only affect the undamaged material. Thus, the damage potential function F^{d} is defined in terms of the effective stresses and strains. By combining plasticity with damage, it seems natural that plasticity can only affect the undamaged material skeleton. Thus the plastic potential F^{p} is originally defined in terms of the effective stresses and strains and subsequently converted to the damaged space. The plastic potential F^{p} and the damage potential F^{d} can have several forms [6]:

$$F^{p} = F^{p}\left(\bar{\sigma}_{ij}, \bar{X}_{ij}, \bar{R}\right) \tag{14}$$

$$F^d = F^d\left(Y_{ij}\right) \tag{15}$$

where $\bar{X}_{ij} = M_{ijkl}X_{kl}$ is the effective backstress tensor and $\bar{R}$ is the effective isotropic hardening.

When considering the damage and plastic deformations of metal matrix composites, we can use the combined damage and plastic formulations for each of the constituents. The information obtained from the individual properties of the different materials at the local level can be linked to the overall properties by using a certain homogenization technique. For further details on the subject consult reference [13], [14], and [15].

6. Conclusions

Described within this work is an experimental procedure by which damage can be quantified in terms of microcrack density. Damage quantification is accomplished through use of a scanning electron microscope and image analyzing software. This equipment is used to measure physical damage features (microcracks) on a representative volume element (RVE) taken from test specimens.

The primary focus of this investigation is to convert physical damage into a mathematically defined damage tensor. Given that physical damage can occur in different forms (e.g. fiber and/or matrix cracks, matrix voids, fiber-matrix debonding, etc.) an expression must be selected to quantify damage in terms of a total quantity irrespective of individual forms or in terms of each individual form. Within this work, damage is quantified in terms of crack density as defined by equation (2). The method of data collection is such that crack densities can be obtained as a total value for the laminate RVE or individual values for the fiber and matrix. Although equation (2) only considers damage resulting from features in the form of cracks, they can be replaced by expressions for other damage features and combined as given by equation (1). Results of this investigation show that physical damage can be quantified into a tensorial quantity suitable for any damage constitutive model.

Additional investigations were conducted [6] using the experimental data presented here in order to verify the formulation for a coupled anisotropic damage model for the inelastic response of composite materials. A physical interpretation of the second order damage tensor, ϕ, is presented in that work.

7. References

1. Allix, O., Ladeveze, P., Gilletta, D. and Ohayon, R. (1989) A damage prediction method for composite structures, *Int. J. Num. Meth. Eng.* **27**, 271–283.
2. Majumdar, B.S., Newaz, G.M., and Ellis, J.R. (1993) Evolution of damage and plasticity in titanium-based, fiber-reinforced composites, *Metall. Trans. Ser. A* **24A**, 1597–1610.
3. Breuing, T.M., Stock, S.R., Kinney, J.H., Guvenilir, A., and Nichols, M.C. (1991) Impact of x-ray tomographic microscopy on deformation studies of a SiC/Al MMC, in *Material Research Society Symposium Proceedings,* Material Research Society, pp. 135–141.
4. Lemaitre, J. and Dufailly, J. (1987) Damage measurements, *Eng. Frac. Mech.* **28**, 643–661.

5. Voyiadjis, G.Z. and Kattan, P.I. (1993) Damage of fiber-reinforced composite materials with micromechanical characterization, *Int. J. Solids Struc* **30**, 2757–2778.
6. Voyiadjis, G.Z. and Deliktas, B. (2000) A coupled anisotropic damage model for the inelastic response of composite materials, *Computer Methods in Applied Mechanics and Engineering* **183**, 159–199.
7. Voyiadjis, G.Z., Kattan, P.I., and Venson, A.R. (1993) Evolution of a damage tensor for metal matrix composites, in *MECAMAT 93 International seminar on micromechanics of materials,* Moret-sur-Loing, France, **84**, pp. 406-417.
8. Lemaitre, J. and Chaboche, J.-L. (1990) *Mechanics of Solid Materials,* Cambridge University Press, London.
9. Carlsson, L.A. and Pipes, R.B. (1987) *Experimental Characterization of Advanced Composite Materials,* Prentice-Hall, Inc.
10. Turtle, M.E. and Brinson, H.F. (1984) Resistance-foil strain-gage technology as applied to composite materials, *Exp. Mech.* **24**, 54–65.
11. Voyiadjis, G.Z. and Venson, A.R. (1995) Experimental damage investigation of a SiC-Ti aluminide metal matrix composite, *Int. J. Damage Mech.* **4**, 338–361.
12. Venson, A.R. and Voyiadjis, G.Z. (2001) Damage quantification in metal matrix composites, *J. Engrg. Mech.* **127**, 291-298.
13. Voyiadjis, G.Z. and Kattan, P.I. (1999) *Advances in Damage Mechanics:Metals and Metals Matrix Composites* , Elsvier, Oxford.
14. Park, T. and Voyiadjis, G.Z. (1997) Kinematic description of damage, *Journal of Applied Mechanics* **65**, 93-98.
15. Voyiadjis, G.Z., and Park, T. (1997) Anisotropic damage effect tensors for the symmetrization of the effective stress tensor, *Journal of Applied Mechanics* **64**, 106-110.